



UNIVERSITÀ
DEGLI STUDI
FIRENZE

FLORE

Repository istituzionale dell'Università degli Studi di Firenze

Cultural heritage microclimate change: Human-centric approach to experimentally investigate intra-urban overheating and numerically

Questa è la versione Preprint (Submitted version) della seguente pubblicazione:

Original Citation:

Cultural heritage microclimate change: Human-centric approach to experimentally investigate intra-urban overheating and numerically assess foreseen future scenarios impact / Pioppi B.; Pigliautile I.; Piselli C.; Pisello A. L. - In: SCIENCE OF THE TOTAL ENVIRONMENT. - ISSN 0048-9697. - ELETTRONICO. - 703:(2020), pp. 134448-N/A. [10.1016/j.scitotenv.2019.134448]

Availability:

The webpage <https://hdl.handle.net/2158/1263889> of the repository was last updated on 2022-04-04T18:29:35Z

Published version:

DOI: 10.1016/j.scitotenv.2019.134448

Terms of use:

Open Access

La pubblicazione è resa disponibile sotto le norme e i termini della licenza di deposito, secondo quanto stabilito dalla Policy per l'accesso aperto dell'Università degli Studi di Firenze (<https://www.sba.unifi.it/upload/policy-oa-2016-1.pdf>)

Publisher copyright claim:

La data sopra indicata si riferisce all'ultimo aggiornamento della scheda del Repository FloRe - The above-mentioned date refers to the last update of the record in the Institutional Repository FloRe

(Article begins on next page)

Cultural heritage microclimate change: human-centric approach to experimentally investigate intra-urban overheating and numerically assess foreseen future scenarios impact

Benedetta Pioppi¹, Ilaria Pigliautile¹, Cristina Piselli^{1,2}, Anna Laura Pisello^{*1,2}

¹CIRIAF Interuniversity research centre on pollution and environment Mauro Felli, via G. Duranti 63, 06125 Perugia, Italy

²Department of Engineering, via G. Duranti 93, 06125 Perugia, Italy

* Corresponding author: anna.pisello@unipg.it

Abstract

Microclimate change related events affect cities total environment and therefore citizens' wellbeing. In a framework of urban resilience challenge, it is important to guarantee thermally comfortable conditions to dwellers in outdoors but also to preserve cultural heritage masterpieces for tourism and local socio-cultural identity. This work couples an innovative field monitoring at multiple scales and a validated numerical modelling effort to identify indoor and outdoor critical conditions at the present time and in the future, according to IPCC climate change forecast scenarios. The authors focused the attention on the overheating risk of Gubbio historical city center, in central Italy. Experimental data analysis highlights the microclimate granularity of the case study with detected temperature discrepancies up to 2.5°C observed at pedestrian height during the hottest hour, i.e. 2 p.m. Collected data are then used to validate the numerical models of (i) the most significant building of the city and (ii) its surroundings to investigate indoor/outdoor thermal comfort stress due to climate change and local overheating. The combined analysis shows that indoor operative temperature reaches 32°C on average in 80 years, compared to the current 29°C value. In the outdoors, apparent temperature increases by about 10°C on 2100, being responsible for a serious threat compromising socio-cultural life, human health and outdoor and recreational activities.

25

26 **KEYWORDS**

27 Urban resilience; Wearable sensing technique; Cultural heritage; Outdoor thermal comfort;
28 Microclimate change; Energy efficiency in building.

29 **1. Introduction**

30 Climate change is considered as one of the most significant hazard of the 21st century [1]. This
31 phenomenon looms as increase in frequency and intensity of extreme weather events [2], such as
32 heat waves, droughts, floods, landslides, cyclones and heavy precipitations in the next future [3].
33 Moreover, anthropogenic actions have been widely acknowledged to be responsible for urban
34 climate alteration, due to land covering modification and greenhouse-gas emissions. The Urban
35 Heat Island (UHI) phenomenon at surface level, i.e. Surface Urban Heat Island (SUHI), which refers
36 to the increase in urban areas surface temperature with respect to the surrounding rural areas, is
37 the evidence of that and it is detected in more than 400 cities worldwide (e.g. Sidney [4], Athens
38 [5], Milan [6], Californian cities [7], Singapore [8] , etc.), and it is responsible for a huge modification
39 of the urban anthroposphere, hydrosphere, biosphere and atmosphere. The analysis of the UHI
40 magnitude show that the UHI intensity can reach 5°C and exceed 8°C [9]. Moreover, synergy
41 between UHI and the increasing frequency, duration and strength of heat waves is demonstrated
42 by Perkins et al [10]. Li and Bou-Zeid show that daytime and nighttime UHI indexes computed during
43 the heat wave period in Baltimore-Washington metropolitan are higher compared to indexes
44 obtained just before the extreme weather event, as demonstrated by means of a combination of
45 observational and modeling analysis [11]. This urban overheating affects the urban livability of the
46 city and it has multiple impacts on energy consumption, environment and pollution, on citizens'
47 health condition and comfort perception, on economy in terms of tourism and human well-being in

48 general [12]. Most of all, urban overheating also involves city centers and dense urban areas,
49 including cultural heritage places, which become increasingly less livable and accessible, with all the
50 consequences on a societal basis. The most documented consequence is the increase of the peak
51 and global electricity demand for heating, ventilation and air conditioning (HVAC) systems.
52 Santamouris et al. examine 30 monitoring profiles of urban and suburban weather stations in
53 Athens, they detect doubled and tripled peak building electricity demand due to UHI [13]. On the
54 other hand, Huang and Gurney quantify the financial implications of climate change to consumers
55 at suppliers and find out energy savings up to 340 \$/years in heating dominated climates, while
56 highlight an increase in energy costs up to 231 \$/years for warmer states in the U. S. [14].
57 Consequences of urban warming include human health threats and influence on mental well-being
58 and human thermal sensation, i.e. heat and cold stress. Numerous studies show the clear correlation
59 between ambient temperature and mortality, suggesting higher risk of mortality in areas with hot
60 or cold temperature and relatively lower rates in optimal temperature zones [15]. From an
61 economic point of view, tourism, recreation and outdoor activities are strongly influenced and
62 deterred by climate [16], [17], and also their resilience may be impact by the lack of visitability due
63 to local overheating compromising outdoor wellbeing in most of the hot season everywhere. Abed
64 et al. study the role of thermal and physical well-being on potential tourism in Algeria and point out
65 how weather and climate are crucially important factors' in tourism potentiality [17]. Moreover, the
66 perception of climate conditions can change in function of tourists' native country and it has been
67 considered by Salata et al., who combine tourism and climate perceptions by using the MOCI and
68 the PMV indices for local and international tourists, respectively, traveling to three Italian cities, i.e.
69 Venice, Rome and Palermo, in order to manage tourist fluxes [18]. In this panorama, to counteract
70 climate change process and the related multidimensional consequences on economy and wellbeing,
71 the scientific communities put in place a huge effort in developing and implementing several

mitigation and adaptation techniques [19]. Among them, the implementation of new materials able to (i) optimize radiative exchanges in terms of solar radiations and environment, i.e. cool roof, cool pavements [20]–[22] or to (ii) store and release solar thermal energy shifted in the time, i.e. phase change materials [23] appear to be very promising or to take advantage from the evapotranspiration contribution [24]–[26], and (iii) the use of greenery, i.e. green roof, presents a high mitigation potential [27]. Moreover, better results are expected and obtained by combining more than a single mitigation strategy, as demonstrated by Mohd Fairuz Shahidan et al. that combine both trees and ground surface materials mitigation technologies and point out a reduction in the average of air temperature by 2.7°C and in the maximum peak by 3.5°C [28]. Despite a huge effort has been done by the scientific community to outline potential climate mitigation strategies, frequently they are not applicable in historical urban context which presents several constraints for its cultural value preservation[30], i.e. any architectural modification is indeed forbidden. Historic urban areas were built for different purposes (e.g. defense issues etc.) and different climatic and demographic conditions, hence their architectural design respects the needs of that era, which often does not meet those of nowadays. For these reasons, the effects of climate change are even more exacerbated in the case of built cultural heritage, since resilience strategies should be investigated in order to preserve urban cultural heritage and even more the livability in city center areas. Moreover, re-use of historic buildings is a common practice nowadays, but the application of active or passive solutions to improve indoor environmental quality is not always feasible due to architectural constrains [31]. Therefore, a continuous monitoring of the indoor conditions is fundamental to ensure comfortable conditions for occupants [32], [33].

Moreover, human well-being perception plays an important role in city context driving dwellers habits and tourists flow [34]. For this reason, outdoor thermal comfort interested researchers for decades [35]. Practical indices have been proposed aiming to: (i) consider the wide variety of

96 microclimatic and physiological parameters which influence the perception of each individual and
97 more in general of the community; (ii) grade thermal sensation in outdoors; (ii) evaluate human
98 conditions in various outdoor conditions [36] Nevertheless, this challenge is an ongoing process [36].
99 The pedestrian perspective is still missing; hence it opens scientific investigation possibility.

100 Within the presented framework, this study proposes an innovative methodology coupling
101 multiscale experimental monitoring and numerical modeling strategies to identify critical conditions
102 in terms of heritage site resilience and dwellers/citizens' wellbeing both at inter-building and single-
103 building dimension. The proposed methodology, deeply described in section 2 of the paper, can be
104 summarized as follows:

- 105 (i) investigation of the existing, site-specific, microclimate conditions in the heritage site, by
106 means of available weather data and collection of additional information thorough usage of
107 stand-alone and easily-to-install thermohygrometers;
- 108 (ii) focus on the pedestrian perspective and assessment of human outdoor and indoor thermal
109 comfort by means of direct and rational comfort indexes calculation;
- 110 (iii) extension of the experimentally-driven analysis to future scenarios through numerical
111 modelling and the adoption of forecasted weather forcing taking into account the on-going
112 process of climate change according to IPCC scenarios.

113 The above-mentioned procedure allows to highlight the most critical areas within a specific case
114 study and to point out potential worsening in comfort perception inside public heritage buildings.

115 The final goal is therefore to address local policy-makers towards tailored strategies to enhance the
116 livability of the site and the preservations of its monuments. The authors present such methodology
117 applied to the city center of Gubbio, a Medieval hilly town in Italy, and more specifically to its most
118 touristic building facing the town main square, i.e. Palazzo dei Consoli. According to the Koppen
119 and Geiger classification [37], Gubbio climate is *Cfb* that stands for temperature climate in the

middle latitude with absence of a dry season and presence of rainfall every month of the year. In general temperatures belonging to this category in the coldest month are higher than -3°C and below 18°C , in addition, at least a month is characterized by air temperature average of 10°C . A detailed description of the case study is given in section 3. Outputs of both the experimental campaigns and the numerical analysis are presented in section 4 and final conclusions and potentials of the method are pointed out in section 5.

Therefore, the novel contribution of the work consists of the integration of a per-se novel environmental monitoring technique that, for the first time, is able to detect the pedestrian perspective on microclimate scenarios in the indoors and outdoors, with classic monitoring campaigns useful for the calibration and validation of numerical models run for climate change prediction scenarios. This technical procedure is then aimed at providing reliable and useful data for policy makers and other stakeholders (public authorities, etc.) who may better understand population fluxes and increase in morbidity related to climate change hazards, responsible for social life modifications in the outdoors. The proposed approach may guarantee a wide replicability potential in dense historical cities, which are often neglected while developing and implementing UHI mitigation techniques and are becoming increasingly less resilient to climate change related events.

2. Methodology

This study aims to present a method for the microclimate investigation of heritage sites coupling in field monitoring and numerical modelling at different scales through the following steps:

- (i) in-field monitoring by wearable systems, specifically designed to this aim,

- (ii) In-field monitoring by local permanent weather stations in key points of the urban contexts
- (iii) Building scale and inter-building scale modelling and calibration thanks to data collection in (i) and (ii)
- (iv) Elaboration of climate change prediction boundaries for both the modelling categories at (iii) and simulation of future climate change forcing scenarios, according to internationally acknowledged reports.

The proposed human-centered evaluation perspective is able to identify indoor and outdoor overheating risk at present and in the next future. The methodology approach is resumed in Figure 1 and the following sub-sections deepen each single step of the work-flow.

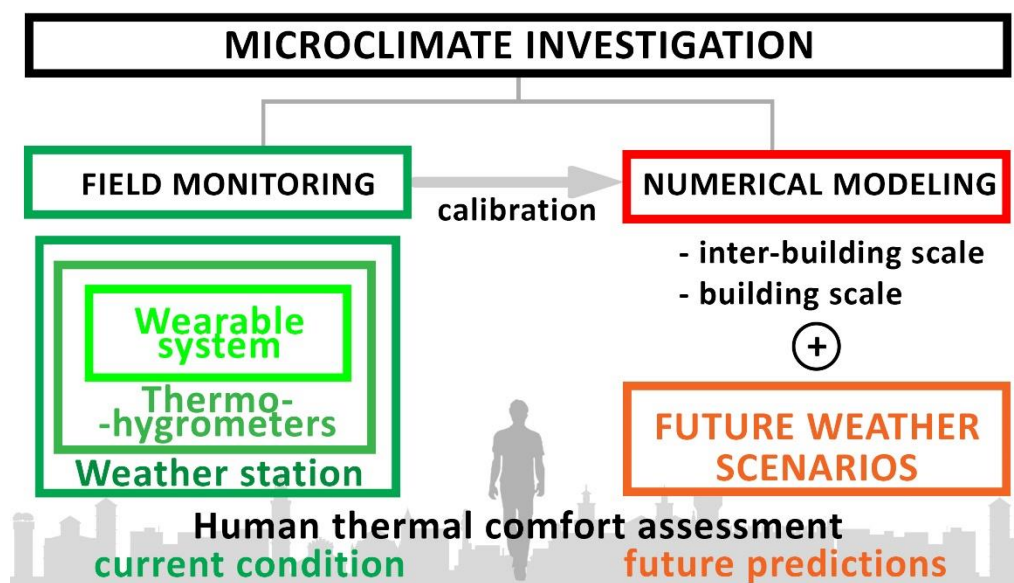


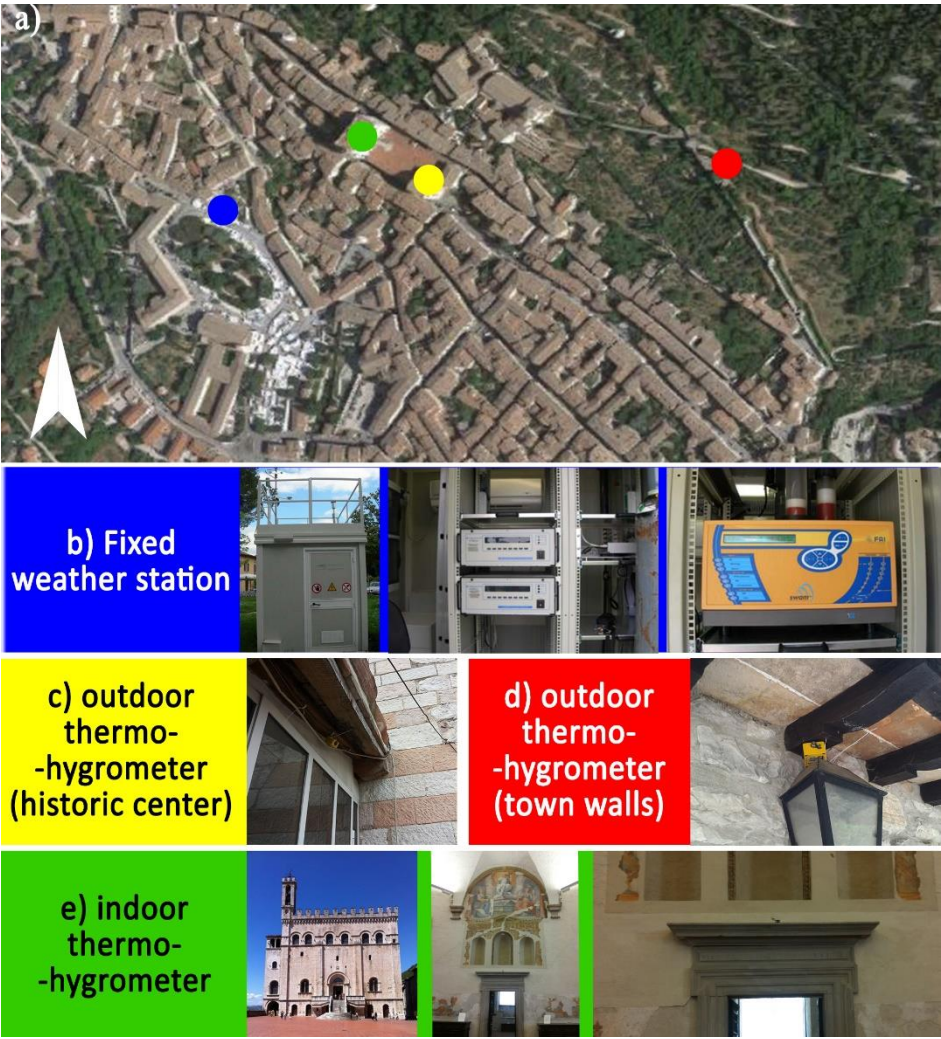
Figure 1 Flow-chart of the applied methodology coupling field monitoring and numerical modeling

2.1 Field monitoring

In order to assess the microclimate variability of the case study, the conducted monitoring campaign integrates different monitoring systems, each one focused on a different scale and perspective of

158 analysis. The adopted systems are: (i) a fixed weather station, (ii) stand-alone thermohygrometer
159 probes, and (iii) a new wearable environmental monitoring system[38] .

160



161

162 *Figure 2. a) site-location of the fixed monitoring system involved in the study: (b) fixed weather station, and (c-d-e) three small air*
163 *temperature and humidity stand-alone probes*

164

165 In particular, the fixed weather station is managed by the regional environmental protection agency
166 and is located at the bottom of the town historic center in a green open field area (Figure 2a, b). The
167 station is equipped by a rain gauge, a barometer, a standard wine vane, a pyrometer, an UV-A and

168 UV-B radiometer and provides reading in hourly resolution. These data are mainly used to allocate
169 site-specific and more frequent data collection into a proper weather history of the area.

170 Two thermo-hygrometers are installed close to two selected areas of the case study which are
171 considered as key tourism spots with specific conditions, as shown in Figure 2c, d. In particular, one
172 probe is located within the historic city center, on the terrace of the municipality building facing the
173 main square of the town, while the other probe is located close to the ancient town walls, at the
174 border between the Medieval city and the surrounding woods. An additional temperature probe is
175 located inside the most tourist-attractive heritage building located on the main square of the case
176 study town (Figure 2e). These points are selected also because they were accessible for
177 maintenance, safe and also representative of specific points that will be later used to correlate and
178 validate microclimate models.

179 The adopted probes are small-size, stand-alone dataloggers (Tinytag model TGP-4500). Such
180 instruments are able to monitor values from -25°C to 85°C in temperature and from 0 to 100% in
181 relative humidity. The recording time-step is settled every 10 minutes to guarantee an internal
182 memory capacity of three months. The installation criteria took into account the necessity to shade
183 all the sensors from direct solar radiation, in order to ensure the reliability of the hygrothermal
184 measurements. Therefore, the sensors are ventilated from roofs and facades in order to not be
185 affected by the close proximity to the built environment.

186 Finally, the focus of the environmental monitoring is turned on the pedestrian perspective to deeply
187 examine and detect critical environmental condition in terms of citizens' well-being. To this aim, a
188 detailed monitoring campaign is conducted by means of an innovative wearable monitoring system.
189 This is a miniaturized weather station able to carry out a multiphysics analysis of the urban and
190 suburban areas from the fragile human perspective. It is composed by a series of miniaturized
191 sensors implemented in a specific designed support which has been properly tailored for being

192 installed over a helmet or on a backpack. Its characteristics of light-weight and small-size allow to
 193 collect weather data and other microclimate parameters along cities transects and other
 194 environment that are not accessible for commonly used transportation vehicles [38]. Moreover,
 195 data collected by such human-centered monitoring device are particularly suitable to get a more
 196 accurate investigation of human thermal perception in outdoors [38].

197 From a technical point of view, the system collects all the parameters reported in Table 1 every 2
 198 seconds. Additionally, it is equipped by an infrared and a visible camera, and a GPS antenna which
 199 allows to link all the collected environmental parameters to their specific location in terms of
 200 latitude, longitude, altitude, and attitude, i.e. roll, pitch and yaw (Figure 3).

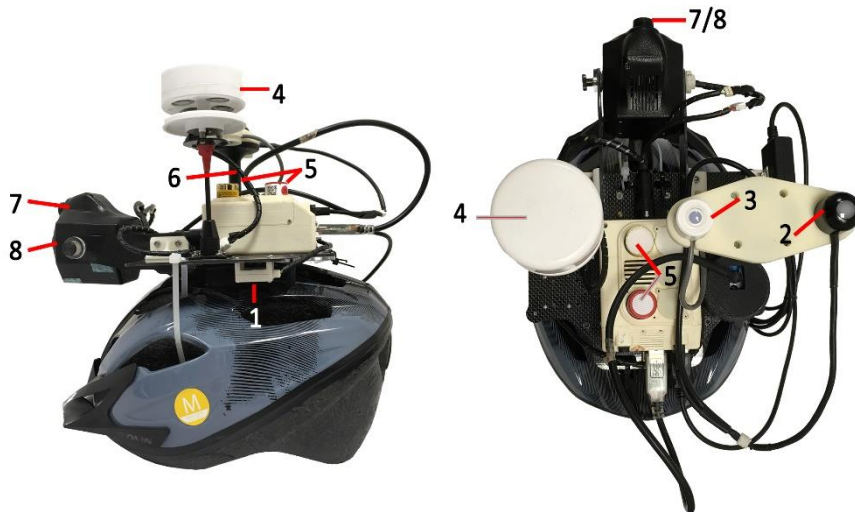
201

Monitored parameter				Technical specifications
Air Temperature [°C]				Absolute accuracy: $\pm 0.5^{\circ}\text{C}$ at 25°C
				Response time: 1s
Relative Humidity [%]				Absolute tolerance: $\pm 3\%$
				Response time: 1s
Atmospheric Pressure [hPa]				Sensitivity error: $\pm 0.25\%$
				Response time: 1s
Global	Solar	Radiation		Spectral range: $360\div 1120\text{ nm}$
[W/m ²]				Calibration uncertainty: $\pm 5\%$
Lighting [lux]				Spectral error: 2.3%
				Response time < 1ms
Wind speed [m/s]				Operational range: $0.25 \div 40\text{ m/s}$
				Resolution: 0.1 m/s
				Sensitivity: 0.13 m/s

	Output rate: 2 Hz
Wind direction [deg]	Resolution: 1°
	Sensitivity: $\pm 1^\circ$
	Output rate: 2 Hz
CO ₂ concentration [ppm]	Accuracy: $\pm 2\%$ full scale
	at 20°C and 1000 hPa
	Response time (T ₉₀): < 30s
CO concentration [ppm]	Measurement range: 0 ÷ 2000
	ppm
	Resolution < 0.5 ppm
	Response time (T ₉₀): < 30s
VOC concentration [kOhm]	Response time (T ₉₀): $\leq 15s$
GPS coordinates	Horizontal spatial accuracy: 2.5m

Table 1 Parameters collected by the innovative wearable monitoring system[38]

The system has also a Wi-Fi access that allow to connect the monitoring system and visualize over real time the collected environmental parameters and to initialize a record session. The outcomes allow to spatially investigate the microclimate variability of the area and to estimate the human well-being of the pedestrian which is one of the main goals of this work.



1)Thermo-hygrometer; 2) Pyranometer; 3) Luxmeter; 4) Anemometer;
5) CO₂/CO/VOC concentration; 6) GPS; 7) Visible camera; 8) Infrared camera

Figure 3. Overview of the designed monitoring system settled upon a common bike helmet

The detailed monitoring campaign is performed in a sunny summer day, i.e. August 2nd and the same pathway is repeated for three times, i.e. around sunrise, around midday and around sunset, in order to have the spatial and temporal variation of the key environmental parameters. For security reasons, since the selected pathways include parks and other potentially dangerous areas to cover during the night-time, the very last measurements are performed around sunset, i.e. 6-7 p.m. Therefore, the night-time data are gathered from simulation, permanent station and sensors that showed a negligible impact in terms of air temperature values.

The chosen pathway (Figure 4) is previously planned in order to pass through different urban spaces in terms of (i) urban geometry, (ii) canyons orientation, (iii) anthropogenic sources, and (iv) greenery. The length of the pathway is walkable in less than one hour and therefore it is assumed that the detected variability of the environmental parameters is only spatially-driven, with negligible time dependency.

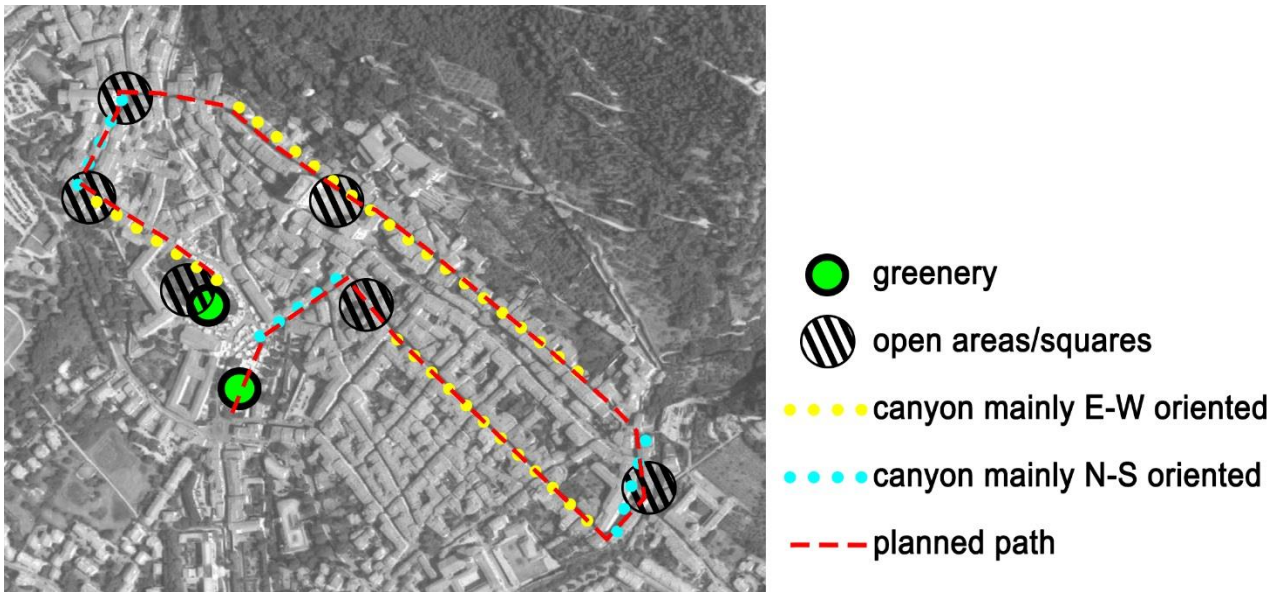


Figure 4 The chosen pathway covered by the wearable system

2.2 Numerical modeling

2.2.1. Numerical microclimate modeling and validation

In order to (i) support the main findings of the experimental campaigns in terms of intra-urban microclimate variability and (ii) extend such findings in time taking into account the main frame of the climate change, microclimate numerical simulations are performed by means of ENVI-met V4 tool, which is a holistic three-dimensional non-hydrostatic simulation engine able to reproduce the microclimatic and physical behavior of urban and rural spaces [39]. The mentioned tool is often used to reproduce and simulate the urban and intraurban environment [40] and it is considered to be the most suitable for the goal of the current work. The model geometry is realized by considering the Arakawa C-grid numerical discretization, both the vegetation and the soil are schematized as one-dimensional column with a certain height and a given respectively leaf and root normalized area density profile. The interaction between the plant and the surrounding air can be provided in terms of direct heat flux, evaporation flux and transpiration flux; while the soil

240 types and surfaces can be assigned for each grid cell considering the individual thermodynamic
241 and hydraulic properties.

242 A global analysis can be carried out and it allows to determine air temperature, relative humidity,
243 global radiation, and mean radiant temperature values within the modeled area [39]. The outdoor
244 air temperature and relative humidity are based on the 3-D wind field which is described as three-
245 dimensional turbulent flow given by the non-hydrostatic incompressible Navier-Stokes equations
246 [41]. Moreover, the distribution of temperature and specific humidity of the atmosphere is
247 controlled by the combined advection-diffusion equation with internal source or sinks [41]. The
248 calculation engine is also able to calculate the radiative fluxes, the incoming shortwave and
249 longwave radiation are calculated by two-stream approximations and some empirical formula [42].

250 The concept of reduction coefficient is used to shape the variation of inside radiation linked to
251 absorption by plants or shading by building [41]. The interaction between the built surfaces and the
252 atmosphere can be carry out considering all the thermos-physical properties as input parameters,
253 i.e. thickness, albedo, thermal emissivity, absorption capability, transmission capability, heat
254 transfer coefficient and heat capacity.

255 In order to get output referring to human perspective, the authors decide to adopt a spatial
256 resolution of 2 m on the three axes, i.e. 2 m units for both horizontal and vertical grids. Due to the
257 adopted constrains, the final model refers only to a portion of the experimentally monitored
258 environment. In particular, the modeled area is centered on the main square of the Gubbio historic
259 center, where the most touristic building faces, and its close surroundings (Figure 5 a). The area is
260 characterized by strong height variation of the terrain, and therefore the elaboration of a specific
261 digital elevation model was necessary to discretize the ground slope. The adopted materials are
262 specifically created in order to faithfully represent the real thermal properties and condition of the
263 area as it is summarized in Figure 5.

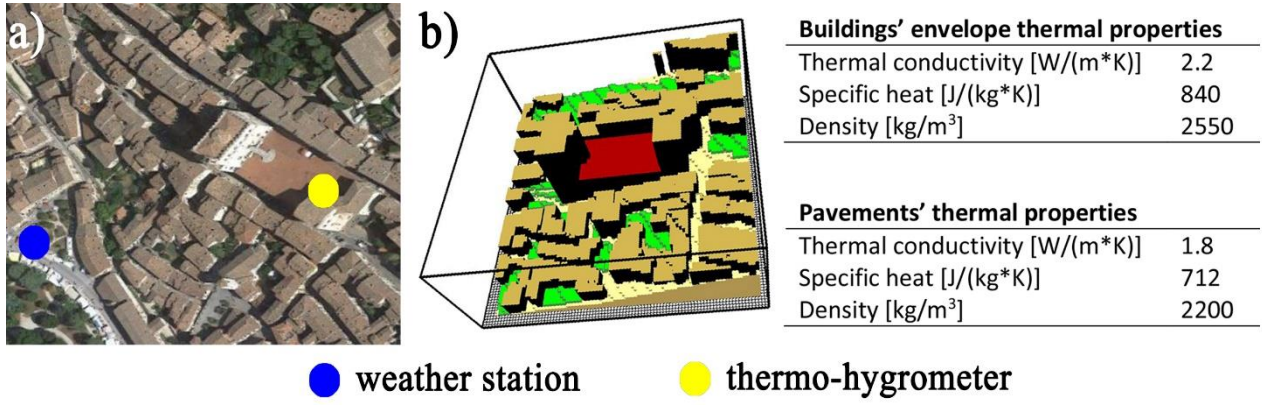


Figure 5 (a) Site locations of references weather data for (b) microclimate model calibration

The data collected by the fixed weather station are used as weather forcing for the simulation in terms of 24 hours air temperature and relative humidity profile and initial wind speed and direction at 10 m height from the ground. The simulation time step is chosen in order to avoid turbulence issues. Hence, the simulation started during the night with weak turbulence condition and the duration of each simulation is 48 hours, in order to provide 24 hours of spin-up (i.e. initialization period for the CFD calculation), reduce any numerical error in the results, and increase the model accuracy [43].

The simulation results are then compared to the observed air temperature data collected by a single thermo-hygrometer in order to validate the models through the calculation of three of the most used calibration indexes [44] which are (i) Mean Bias Error, and (ii) Root Mean Square Error computed accordingly to the following equations:

$$MBE = \frac{\sum_{j=1}^{N_D} (P_j - O_j)}{N_D} \quad (1)$$

$$RMSE = \frac{\sum_{j=1}^{N_D} (P_j - O_j)^2}{N_D} \quad (2)$$

where P_j and O_j are the model-predicted and observed variables for each j -th instant and N_D is the number of analyzed data.

282

283 2.2.2. *Dynamic thermal-energy model of the heritage building*

284 In order to evaluate tourists' indoor thermal perception in heritage buildings, the thermal-energy
285 model of the most attractive historical building of the case study is developed within EnergyPlus
286 simulation environment [45]. The model (Figure 6) takes into account the real geometry and
287 materials thermo-physics properties of the historical building. Therefore, the joint of floors
288 characterized by different heights is realistically modelled, yet avoiding architectural finishes that
289 are not relevant for the purposes of the thermal-energy simulation. In details, the external opaque
290 envelope is characterized by thermal conductivity equal to 2.2 W/m K, density equal to 2550 kg/m³
291 and specific heat equal to 840 J/kg K. As for the occupancy, the acknowledged UK NCM (National
292 Calculation Method for Non Domestic Buildings) [46] standard model for Museums and similar
293 buildings is considered by varying the activity in each thermal zone according to the real end-use,
294 e.g. services, reception, display and public areas, circulation areas, etc. The occupancy density is
295 defined according to the real average occupancy of the building. Therefore, the model is calibrated
296 by means of air temperature data collected by a stand-alone probe that was installed in the main
297 hall of the building for one month.

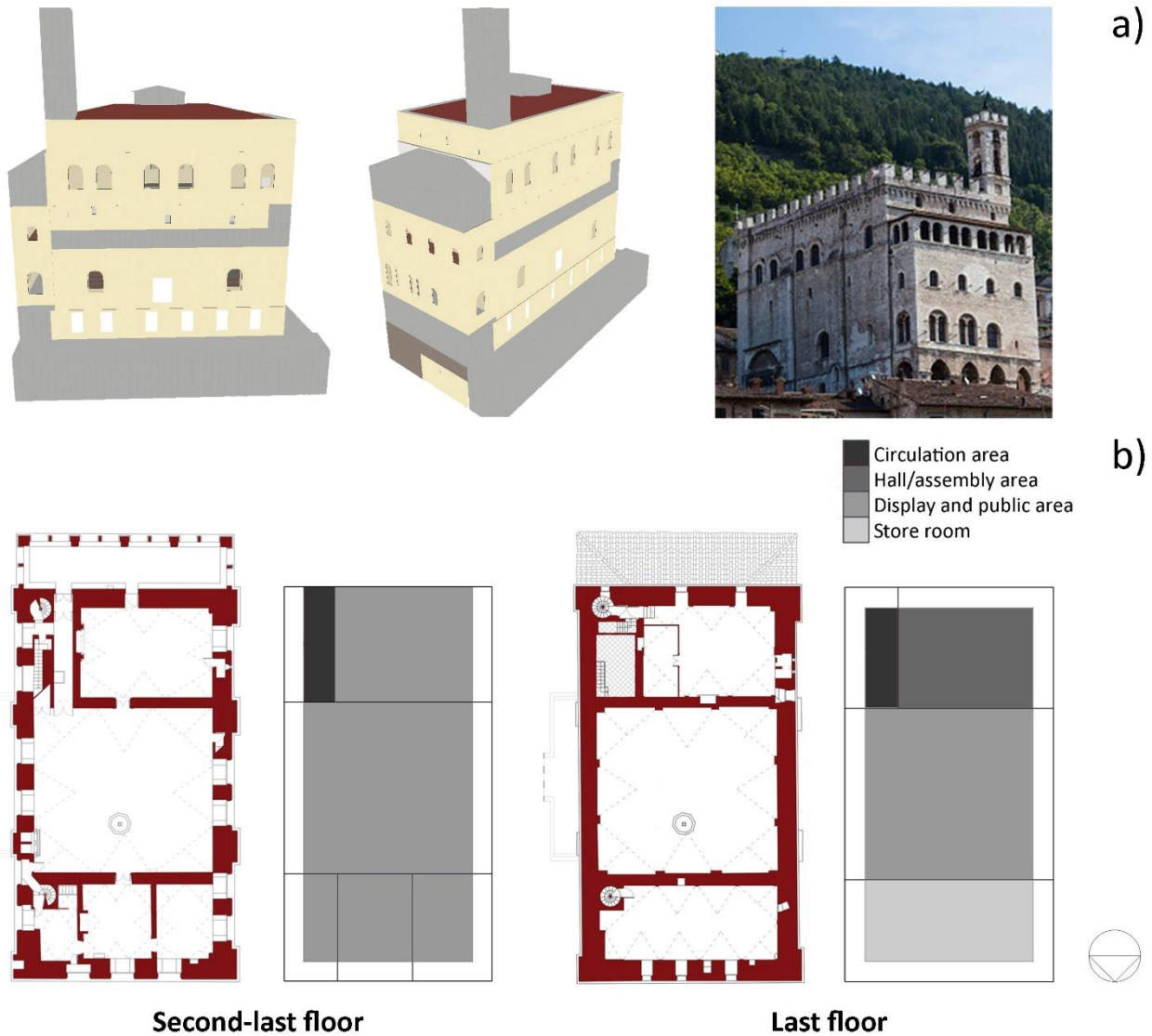


Figure 6 The thermal-energy model of Palazzo dei Consoli: (a) 3D view vs. picture of the building and (b) plan of the two main display and public floors vs. real building plans

The model validation procedure involves the calculation of the same indexes adopted for the validation of the microclimate model, i.e. MBE and RMSE.

Moreover, the outcomes are analysed in terms of operative temperature, which allow to assess the thermal comfort of the occupants in buildings. This parameter, indeed, describes the combined effects of convective and radiant heat transfer. Accordingly, it can be calculated by means the following equation [47]:

$$T_o = \frac{h_r T_{mr} + h_c T_{db}}{h_r + h_c} \quad (3)$$

where h_c and h_r are convective and linear radiative heat transfer coefficient, T_{db} is dry bulb air temperature, and T_{mr} is mean radiant temperature.

2.3. Future climate change prediction scenarios

To analyse how climate change from the past to the future can influence the human thermal comfort perception, four weather forcing scenarios are created by means of Meteonorm tool [48] [49], i.e. a database containing global meteorological and climatological data collected by over 8300 measuring weather stations with reliable detail of solar radiation, five geostationary satellites and a global calibrated aerosol climatology. This tool is able to generate accurate and representative typical years for any place, since it generates site specific weather data thanks to sophisticated interpolation models based on the data collected by the nearby weather stations and on more than 30 years data collections [50]. Moreover, the same tool allows to simulate future climate change scenarios according to the International Panel on Climate Change IPCC prediction; in detail in this work three future weather forcing are created according to the scenario A2 described by the IPCC [51], which is the worst one that demonstrates the best reliability prediction in the past 10 years. It forecasts a slow growth of the share capital, slow technological progress, limited social interaction, economic and cultural differences between regions, an uneven economic growth where the gap between industrialized countries and developing countries is wider, increased soil erosion and water pollution, increased global warming and rising sea level [52]. The selected years for the analysis are 2020, 2050 and 2100. Moreover, a past scenario taking into account as irradiation period 1991-2010 and as temperature period 2000-2009, is created in order to have a reference data. Therefore, in order to investigate how climate change influences human well-being, especially during summer

331 which is the most touristic season of the year and the most delicate due to overheating risk, typical
 332 summer days are selected for each year in order to run the microclimate simulation and analyse the
 333 human thermal comfort perception by PET computed by Rayman model [53], [54] .
 334 Firstly, the entire summer period, i.e. from June 21st to September 21st, of the created weather files
 335 are analysed in terms of cloud cover and air temperature trend in order to select a typical summer
 336 day characterized by clear sky conditions and the mean hottest air temperature. Cloudless sky days
 337 are preferably chosen, since the adopted simulation tool may be considered as mostly reliable under
 338 stable atmospheric conditions. The extreme values of air temperature and relative humidity for the
 339 chosen days are listed in Table 2.

340

Year	Air Temperature [°C]		Relative Humidity [%]	
	Maximum	Minimum	Maximum	Minimum
Past (2000-2009)	34.9	22.0	85.5	47.8
2020	34.6	23.5	84.5	46.2
2050	36.0	23.7	93.6	43.6
2100	38.8	29.8	97.4	52.9

341

342 *Table 2 Extreme values of air temperature and relative humidity for the chosen days*
 343

344

344 These weather files are then used as input forcing to run the microclimate simulation environment
 345 and to conduct accurate analysis about the relationship between climate change and human well-
 346 being in the outdoors.

347

348 *2.4 Outdoor thermal comfort analysis*

349 In order to evaluate how changes in urban thermal environment can affect human well-being, the
350 Apparent Temperature (AT) as well as the Physiologically Equivalent Temperature (PET) are
351 calculated.

352 The apparent temperature is defined as *“the temperature at the reference humidity level producing*
353 *the same amount of discomfort as that experienced under the current ambient temperature,*
354 *humidity, and solar radiation”* [55]. It is a direct comfort index, i.e. directly driven upon
355 environmental data, and it is therefore computed for both the monitored actual conditions and the
356 simulated future scenarios. Essentially, it is an arrangement of the air temperature based on the
357 humidity level and the wind chilling effect, but it does not include the solar radiation contribute in
358 the formula adopted in the current work since the human body net radiation is not an available data
359 according to the monitoring system configuration. The formula to calculate this index is reported
360 below (4) and it is applicable to hot weather conditions [56], [57] :

$$361 \quad AT = T + 0.33 \cdot vp - 0.7 \cdot v - 4.0 \quad (4)$$

362 Where, T is the dry bulb temperature, v the wind speed and vp the water vapor pressure in hPa
363 obtained from monitored temperature (T) and relative humidity (RH) through equation (5):

$$364 \quad vp = \frac{RH}{100} \cdot 6.105 \cdot \exp\left(17.27 \cdot \frac{T}{237.7+T}\right) \quad (5)$$

365 The physiologically equivalent temperature (PET) is a rational index which takes into account all the
366 basic thermoregulatory processes of the human body. More in details, PET is based on the thermo-
367 physiological heat balance model called Munich energy balance model for individuals (MEMI) [58].
368 It is applicable to a wide range of real outdoor conditions and is defined by the energy balance
369 equation of human body (6):

$$370 \quad M + W + R + C + E_D + E_{Re} + E_{Sw} + S = 0 \quad (6)$$

371 where, M is the metabolic rate (internal energy production), W the physical work output, R the net
 372 radiation of the body, C the convective heat flow, E_D the latent heat flow to evaporate water into
 373 water vapor diffusing through the skin, E_{Re} the sum of heat flows for heating and humidifying the
 374 inspired air, E_{Sw} the heat flow due to evaporation of sweat, and S the storage heat flow for heating
 375 or cooling the body mass [58]. Each term of the equation is expressed in Watt and can assume
 376 positive or negative value in case of, respectively, power gains or losses for the body. The individual
 377 heat flow is influenced by environmental parameters, i.e. air temperature (influencing C and E_{Re}),
 378 relative humidity (influencing E_D , E_{Re} , E_{Sw}), wind speed (influencing C and E_{Sw}), mean radiant
 379 temperature (influencing R) [58].

380 According to the literature, PET neutral sensation is adapted to different climates [59] and the most
 381 suitable range for the presented case study is the one shown in Table 3 referring to costal
 382 Mediterranean climate with a neutral zone between 20°C and 25°C, as find out from Cohen et al. in
 383 [60].

Thermal sensation	PET range value [°C]
Very cold	$PET \leq 4$
Cold	$4 < PET \leq 8$
Cool	$8 < PET \leq 13$
Slightly cool	$13 < PET \leq 18$
Neutral	$18 < PET \leq 23$
Slightly warm	$23 < PET \leq 29$
Warm	$29 < PET \leq 35$
Hot	$35 < PET \leq 41$
Very hot	$PET > 41$

385

386

Table 3 Thermal sensation and corresponding PET range for costal Mediterranean climate.

387

388 In the current study, the PET thermal index is computed starting from the output of microclimate
389 simulation data. In particular, PET is calculated by means of the RayMan [61] calculation tool by
390 taking into account air temperature, relative humidity, wind speed, short and long radiation fluxes,
391 and the thermo-physiological data of a standard young man whose characteristics are resumed in
392 Table 4, during the course of the simulated time and within the simulated area.

393

Height	Weight	Age	Cloths insulation	Activity
1.75 m	75 kg	35 years	0.5 clo	Walking, 2.5 met

394

395 *Table 4 Subject characteristics for PET calculation*

396

397 Concerning indoor comfort perception, the estimation of overheating risk for visitors of the most-
398 attractive heritage building of the case study is carried out in terms of frequency of simulated hourly
399 air temperature data above comfortable limits during summer season. Particular attention is
400 dedicated to the overheating risk above 30°C, considered as a key threshold affecting human
401 wellbeing [62], [63].

402

403 **3. Description of the case study**

404 Gubbio is a small ancient town located in central Italy (43° 35' N, 12° 57'E) in the North-Eastern area
405 of Umbria Region in Italy centre, which is mostly mountainous, bounded on the east by Apennine
406 mountains and by the Tiber Valley on the west. The urban configuration is typically Medieval with
407 quite narrow urban canyons, i.e. aspect ratio varying between 1.0 and 0.3, and the materials
408 adopted are mainly local stones and terracotta tiles for roofs, i.e. arenaria and bricks.

409 Palazzo dei Consoli is the most important historic monument of the city, designed by Angelo da
410 Orvieto. It was built at the heart of the city in the early 1300s. It is composed by seven floors and
411 characterized by high thickness of the walls, such as ancient buildings, in limestone material, while
412 the floor is realized by terracotta material. Its key city value is also motivated by the fact that it faces
413 the main square of the city where all the main city events usually take place and most of the tourism
414 flux is concentrated.

415 The façade facing the square is divided into three parts by four buttresses. A central fun-shaped
416 staircase leads to the doorway which is flanked by mullioned windows. The upper floor features six
417 arched windows coupled in pairs and adorned with denticulate frames. The top is finished with
418 arches and Guilfe merlons, while on the left there is the battlement bell-tower [64]. The building
419 further peculiarity is that it stands on the mountain slope, hence its foundations were laid on two
420 different level because of the nature of local topography. The difference in altitude between the
421 two levels of the case study area corresponds to 48 meters, starting from an altitude of 501 meters.

422 In this framework, the study focuses on the area surrounding Palazzo dei Consoli to evaluate
423 outdoor and indoor thermal condition especially for tourists and visitors, even under future climate
424 change expected forcing.

425 The climate of Gubbio is *Cfb* according to the climatic classification proposed by Koppen and Geiger
426 [37] which is based on predetermined values of temperature and precipitation calculated according
427 to yearly averages or individual months. The letter *C* means temperate climate in the middle
428 latitude, with balanced heating and cooling prevalence in winter and summer, respectively. The
429 letter *f* indicates the absence of a dry season and highlights presence of rainfall every month of the
430 year. Finally, letter *b* refers to the temperature of the hottest summer month [37].

431

4. Results

4.1 Microclimate field analysis

In this section, all the experimental data collected by means of different monitoring systems are analyzed and integrated. As specified in section 2.1, data involved in the study are (i) the long-term environmental parameters daily profiles extracted from the fix weather station, (ii) time-series of air temperature and relative humidity collected in different and distinctive areas of the case study by means of fix small-size and stand-alone probes, and (iii) the spatial distribution of the main environmental parameters collected during summer overheating monitoring campaign through the wearable, miniaturized system. The integration of these information allows to progressively deepen the assessment of the climatic conditions of the case study with respect to the pedestrian perspective, and therefore to identify the resilience of the historical site with respect to climate change in both the indoors and outdoors.

In detail, Figure 5Figure 7.a reports the daily air temperature data recorded during summer 2017 by the fix weather station. Air temperature trend shows that the selected day for the wearable monitoring campaign, i.e. August 2nd 2017, is within the hottest week of the season, registered during a heat wave event. Therefore, this chosen day can be considered as representative of urban overheating risk.

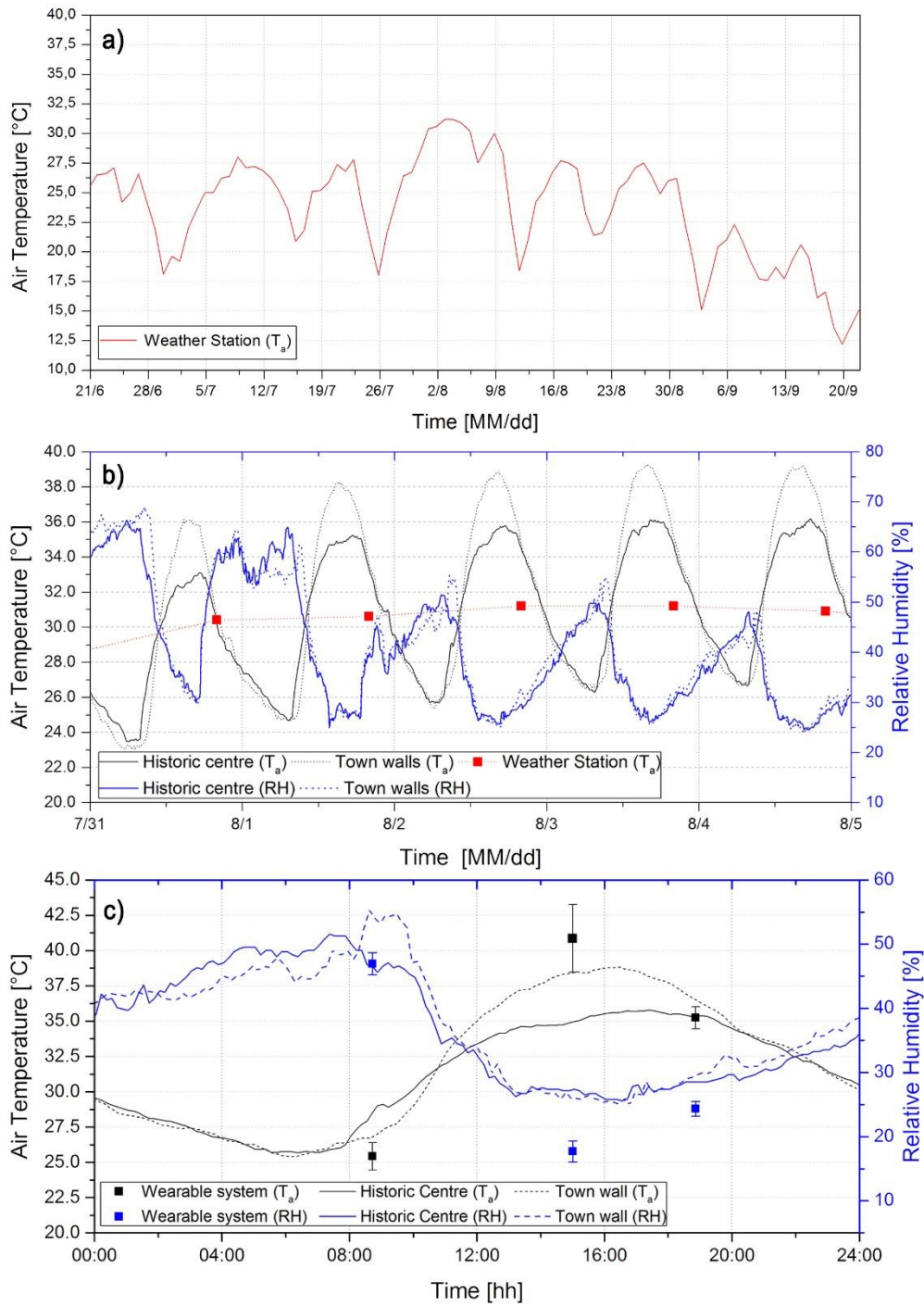


Figure 7.a.b.c.d air temperature summer season trend gathered by the fixed weather station located in Piazza Quaranta Martiri (a), weekly air temperature profiles carried out by the two thermohygrometers and the fixed weather station (b), daily air temperature profile by the two thermohygrometers overlapped to the mean air temperature values recorded by the wearable system(c)

Figure 7.b shows air temperature and relative humidity values gathered, from July 31st to August 5th, every 10 minutes by the two fix small probes, installed on the terrace of the city municipality

456 building (city center area) and on a private garden house (in the city walls area), respectively. The
457 monitored fluctuations in the two analyzed areas are similar in terms of relative humidity profiles,
458 on the contrary they present a significant deviation in terms of air temperature trends. In particular,
459 air temperature profiles differ up to a maximum of 3.6°C observed at 3 p.m. when data collected in
460 proximity of the town-wall are higher. Moreover, temperature inside the city, i.e. measurement
461 point on the terrace of the municipality building, assumes the highest values at night up to 2.8°C of
462 difference with respect to town-wall temperature reached at 8 a.m.

463 Since the used small probes have the same technical characteristics and they are both shielded from
464 the direct solar radiation and of course they were previously calibrated, these values deviations may
465 be directly imputable to site-specific conditions. Such conditions could be related to the actual wind
466 field and/or solar radiation access to the two sites which contributes to generate peculiar
467 microclimatic conditions even in the same small-scale urban area.

468 The relation between site-specific morphology and microclimate conditions is deepened through
469 the environmental investigation by means of wearable sensing techniques. Figure 7.c presents the
470 outcomes of the wearable monitoring campaign conducted at three different times in the same day,
471 i.e. 8 a.m., 2 p.m., and 6 p.m. on August, overlapped to the small probes recorded trends. In
472 particular, each monitoring session by the payload, is resumed by the mean air temperature value
473 and its standard deviation in terms of error-bar length. This comparison highlights the necessity to
474 perform coupled monitoring, i.e. by means of wearable techniques and classic weather stations,
475 since the special granularity of the collected data may be of interest for better understanding the
476 pedestrian perspective.

477 The average air temperature and relative humidity values at pedestrian level follow the daily time-
478 trend recorded by the fix probes. Nevertheless, the amount of data available from the wearable
479 system depicts a variability of the collected environmental signals which is not appreciable from the

480 small probes data. In particular, standard deviation associated to air temperature data reaches up
481 to a maximum of 2.5°C at 2 p.m. which highlights a significant fluctuation of this parameter along
482 the specifically monitored transect. Such variation highlights the intra-urban microclimate
483 diversification due to morphological differences of the crossed dense urban areas, i.e. different
484 orientation and aspect ratio of canyons, presence or absence of greenery, direct solar availability,
485 etc. In fact, the monitoring perspective in this case switches from the urban canopy layer to, more
486 specifically, the pedestrian height. Such perspective is the most representative to evaluate human
487 thermal wellbeing related data.

488

489 *4.2 Numerical modelling*

490 *4.2.1 Calibration and validation of the microclimate model*

491 The reliability of the realized microclimatic model of the case study area is tested by calculating the
492 MBE and RMSE calibration indexes as previously described. According to data availability and
493 general weather conditions, the selected day to compare the observed field measurement by field
494 monitoring and the simulation results was chosen to be December 1st. The validation procedure
495 takes into account simulated and observed air temperature profiles obtained during December 1st,
496 as shown in Figure 8. Through a calibration procedure, MBR and RMSE indexes obtained are equal
497 to 0.2°C and 0.7°C, respectively. According to the literature and the research effort over the last
498 decade, the obtained indexes outcomes can be considered acceptable [39]. The maximum
499 difference in between measured and simulated air temperature values is 1.5°C. The maximum is
500 registered at peak time as expected since the model does not specifically represent a specific point
501 which is the measured point. Therefore, it can happen that the measured peak time may be higher
502 than the average simulated one within the framework of the cell.

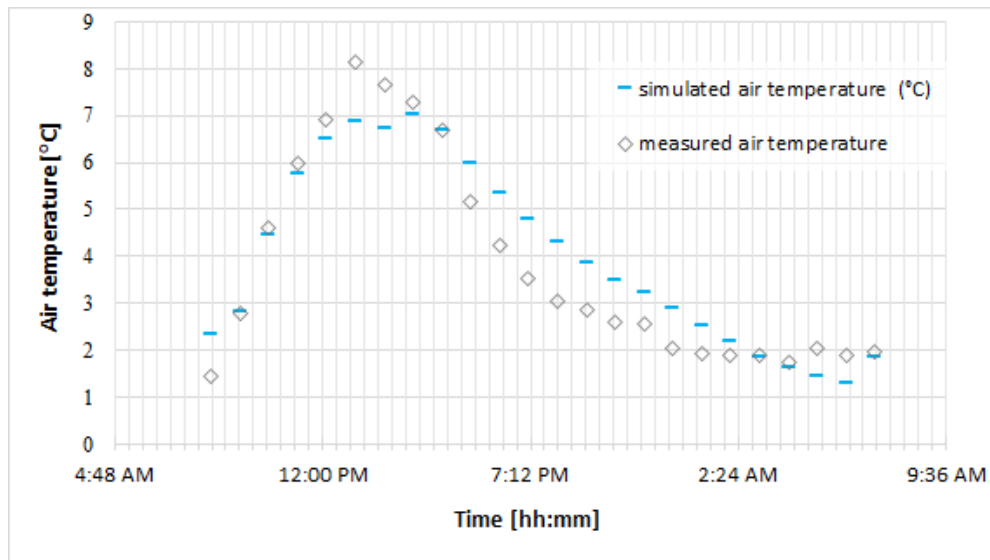


Figure 8 Comparison between measured and simulated air temperature trend

4.2.2 Calibration and validation of the heritage building thermal-energy model

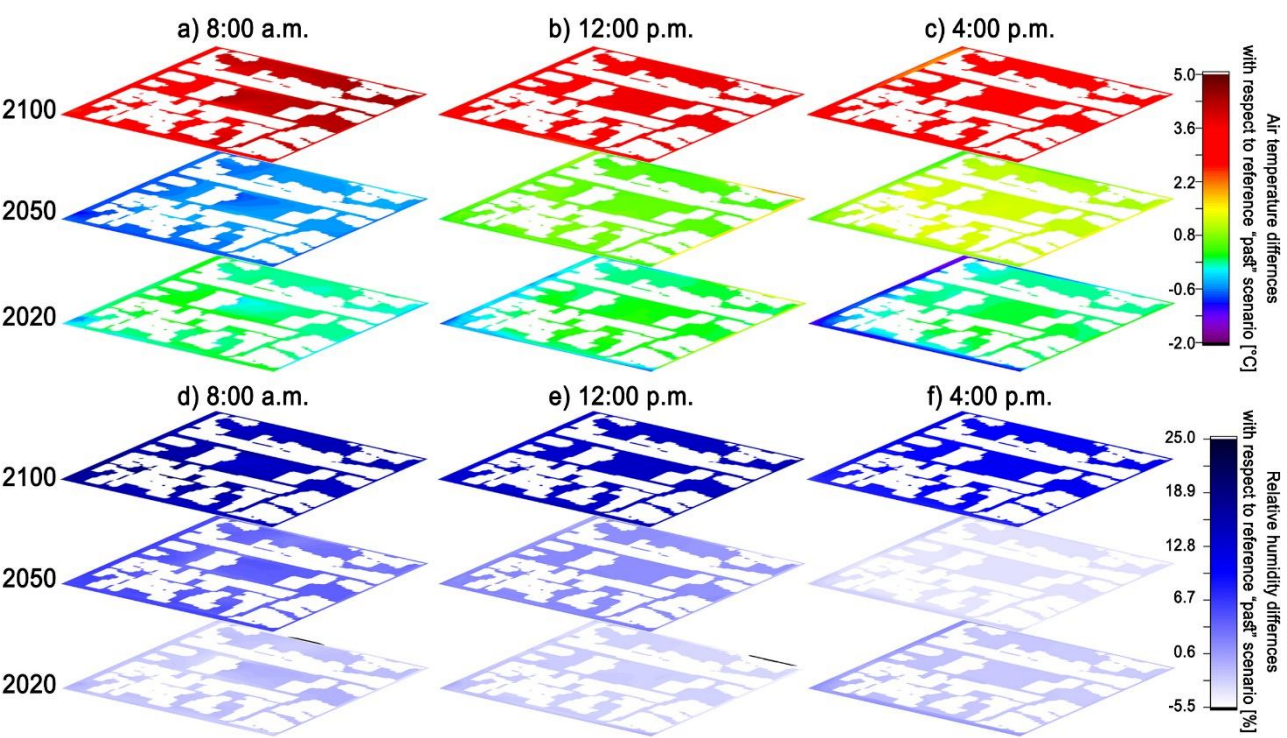
Simulated and measured air temperature profiles are compared also for the single building model reliability in predicting the thermal behavior of the heritage building object of the study. The final obtained MBE and RMSE are respectively 0.33°C and 1.07°C. Such results allow to consider the model as acceptable for the scope of this analysis.

4.2.3 Microclimate analysis of future scenarios

Maps of Figure 9 (a-c) show air temperature differences between the forecasted future scenarios, i.e. 2020,2050,2100, and the reference one for the modelled area during a typical summer day. The spatial distributions at pedestrian level, i.e. 1.10 meters above the ground, are carried out for three representative moments of the selected day: early in the morning, i.e. at 8.00 a.m., at the time of maximum solar radiation, i.e. 12.00 p.m., and at the time of air temperature maximum peak, i.e. at 4.00 p.m. A linear overheating trend, from the past scenario to the furthest future scenario, i.e.

2100, is clearly detectable. The highest air temperature difference is expected in summer 2100 when an average increase by 3.8°C, 3.6°C, and 3.4°C is obtained at 8 a.m., 12 p.m., and 4 p.m. respectively.

523



524

525 *Figure 9 Air temperature (a-c) and relative humidity (d-e) differences between forecasted scenarios, i.e.2020,2050,2100 and the*
526 *reference scenario in summer*

527

528 The same spatial analysis between the foreseen summer future scenarios, i.e. 2020,2050, 2100 and
529 the summer reference one are conducted in terms of relative humidity differences. As illustrated in
530 Figure 9 (d-f), the relative humidity parameter, contrary to the air temperature profile, presents a
531 nonlinear trend from the past reference scenario to the furthest future one, i.e. 2100.

532 More specifically, in summer 2020 as the temperature increases, a decrease in relative humidity is
533 observed. On the contrary, an increase in air temperature corresponds to an increase in relative
534 humidity level in 2100. The maximum relative humidity variation is detected early morning, i.e. 8.00

535 a.m., in 2100 and it is equal to 15%. This singular behavior highlights the tropical-like increasing
 536 climate trend of the case study area, which makes this analysis even more urgent with the purpose
 537 to identify the cultural heritage resilience to climate change related events.

538 All the above-observed changes in terms of air temperature and relative humidity between the
 539 reference past and the future scenarios are not related to site-specific morphologies, but allow to
 540 identify the urban scale boundary conditions at the canopy level of the current case study within
 541 the framework of predicted climate change. A spatially averaged value of the outlined differences
 542 can be considered as representative of the forecasted climate change of this area. Therefore, air
 543 temperature and relative humidity spatially-averaged differences between future scenarios and the
 544 reference one are summarized in Table 5.

	ΔT , summer			ΔRH , summer		
	8 a.m.	12 p.m.	4 p.m.	8 a.m.	12 p.m.	4 p.m.
2020	0.1	0.2	0.0	-1.7	-2.5	-1.9
2050	-0.6	0.6	1.1	3.9	1.3	-3.6
2100	3.8	3.6	3.4	15.5	14.0	10.2

546
 547
 548
 549
 550

Table 5 Spatially-averaged air temperature and relative humidity differences between future scenarios and the reference one at three selected hours, i.e. 8 am., 12 p.m., and 4 p.m.

551 Cities like the one object of the current study, i.e. almost at the same latitude, are going to
 552 experience hotter and more humid summer according to IPCC. These critical conditions threat
 553 citizens and tourists well-being in outdoors and therefore a detailed analysis of the human thermal
 554 comfort perception is presented in the following session.

555

556 *4.3 Tourist comfort analysis*

557 This section is focused on the results of experiments and simulations conducted both in indoors and
558 outdoors, from a pedestrian point of view. The outcomes can be applied to any person living
559 outdoor or indoor, i.e. citizens or tourists. Even though, since Gubbio is a very touristic area and
560 tourists can affect the whole city economy and its resilience to climate change, the current study
561 focused the attention on the tourist perspective.

562

563 *4.3.1 Comfort mapping by means wearable system*

564 This section is focused on the experimental wearable campaign results. In detail, the apparent
565 temperature is calculated in order to assume the human thermal perception during a hot summer
566 day in Gubbio historical urban environment.

567 The obtained results are spatially plotted (color scale) with respect to the global solar radiation
568 values by means plot size, as shown in Figure 10.

569

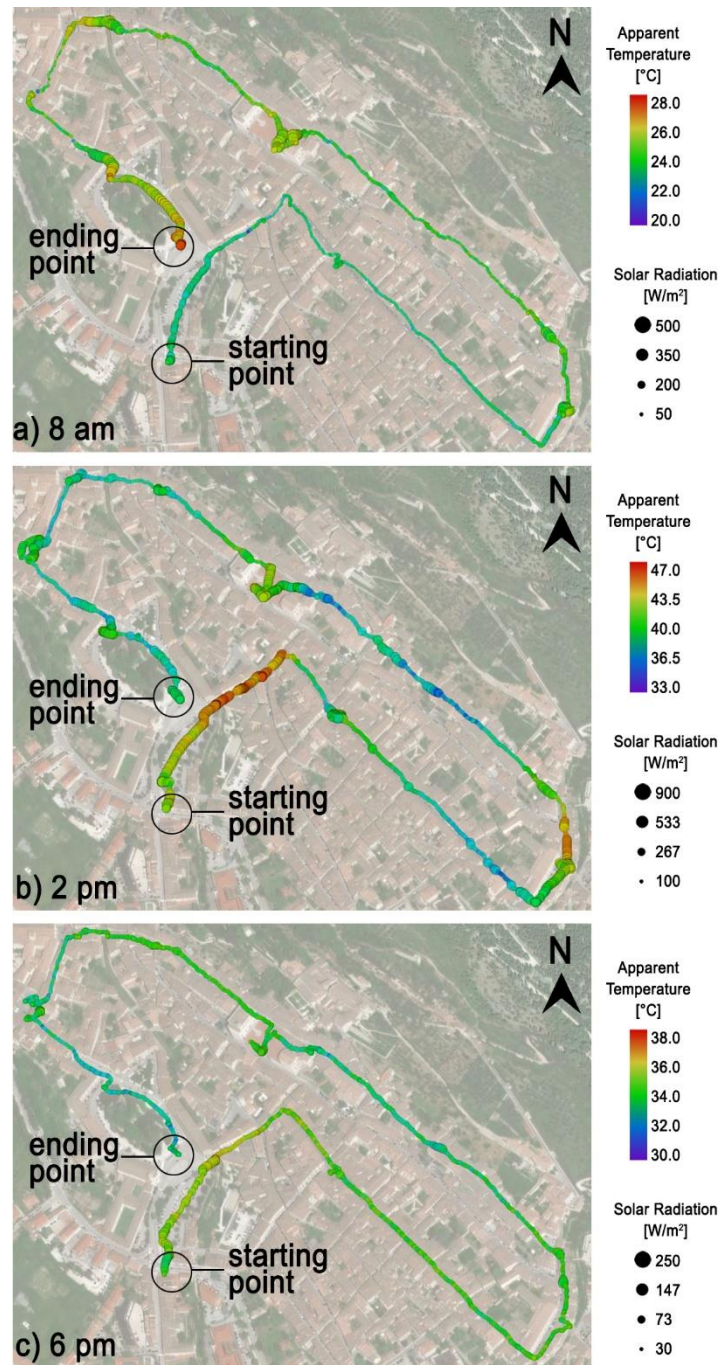


Figure 10 Apparent temperature and global solar radiation maps obtained by means experimental wearable campaign at 8 a.m. (a), 2 p.m. (b), 6 p.m. (c)

As can be seen (Figure 10.a), at 8 a.m. the apparent temperature ranges between 20.10° C and 26.75°C. The maximum values are recorded at the end of the monitoring session when the global solar radiation is supposed to naturally increase, while the minimum ones are registered at the beginning of the survey campaign, which lead to consider a sort of further time dependence.

578 However, the spatial distribution of the apparent temperature values is strictly influenced by the
579 urban morphology patterns. In fact, the highest values are gained around squares on the route
580 where sky view factor and incoming global solar radiation assume higher values. Nevertheless,
581 apparent temperature outcomes show acceptable thermal comfort condition which not lead
582 dwellers or tourists to any health hazard all along the monitoring pathway at this moment of the
583 day.

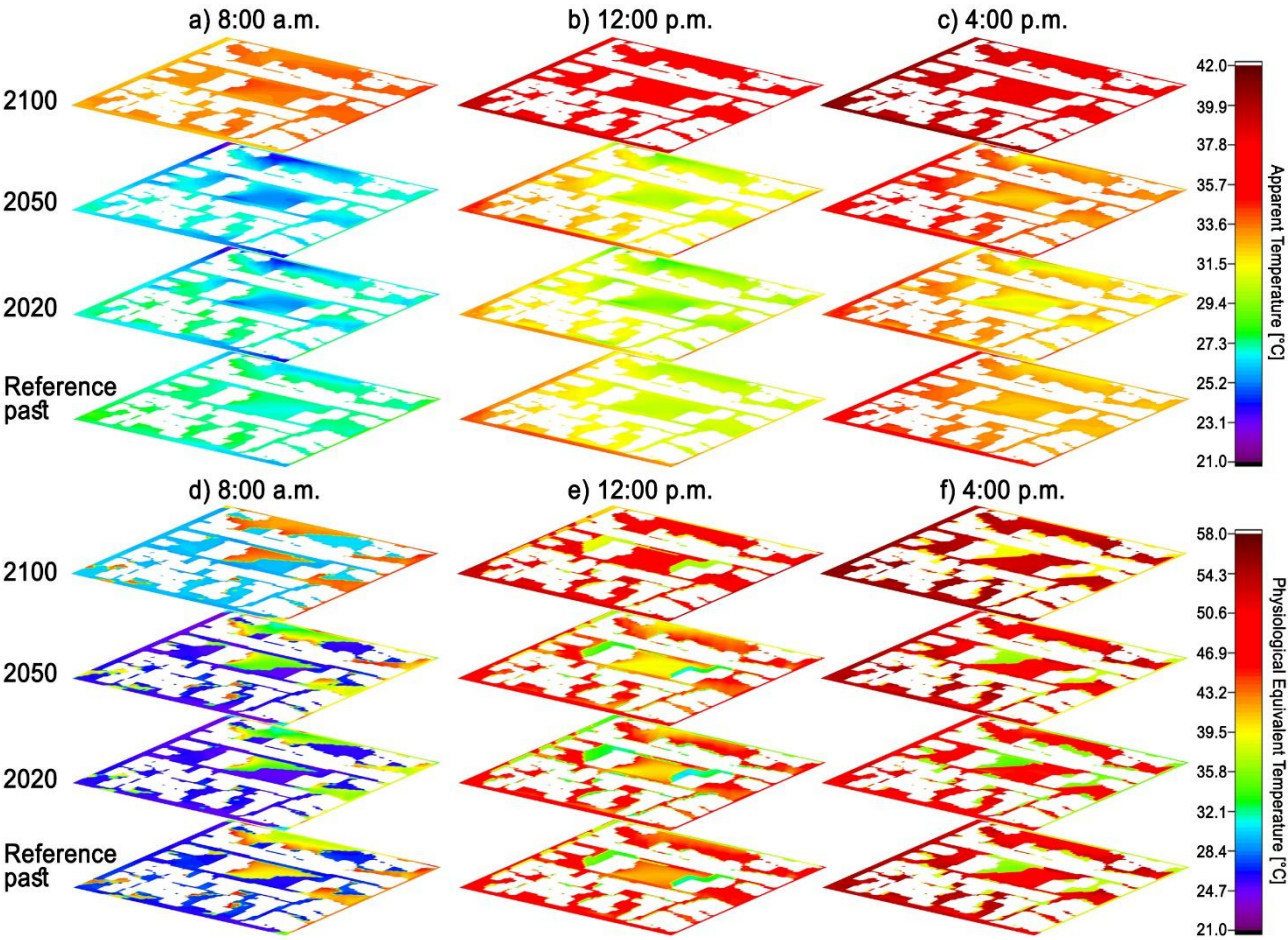
584 On the contrary, at 2.00 pm the apparent temperature rises up to 46.7°C. As shown in Figure 10.b,
585 the most critical areas (which presents the highest apparent temperature values) are the North-East
586 and South-West oriented canyons, mainly facing the slope toward the southern valley. This
587 orientation allows the direct incoming radiation to access the canyon up to the pedestrian level
588 while high aspect ratios of the same streets limit the energy exchanges towards the sky of both
589 reflected shortwave and re-emitted longwave radiation. This trapping effect leads to an increase of
590 the air temperature. Moreover, the wind chill effect is reduced within packed urban areas.
591 Combination of both the altered radiative budget and the reduction of the convective contribution
592 is responsible for higher human thermal stress perception, i.e. higher apparent temperature values
593 as shown in the plots.

594 Finally, at 6 p.m., a general decrease of the global solar radiation is detected. Less intense incoming
595 solar radiation leads to smoother fluctuations of air temperature along the monitoring pathway and
596 the monitored built environment looks more homogeneous in terms of air temperature. This thesis
597 is confirmed by the experienced range of apparent temperature, which is equal to 8°C as well as the
598 apparent temperature variation detected at 8 a.m. However, the detected minimum values
599 corresponded to 30°C, versus 20°C, i.e. minimum value at 8 a.m. This is imputable to the urban
600 fabrics configurations and materials that are overheated during the day and tends to slowly release
601 all the stored heat, due to their thermal capacity.

602

603 4.3.2 Outdoor Thermal comfort perception: actual conditions and future forecast

604 Thanks to data availability, Figure 11 shows the spatial distribution of the calculated apparent and
605 physiological equivalent temperature during the hottest summer day as it is foreseen by the IPCC
606 forcing scenarios.



608 Figure 11 Spatial distribution of apparent temperature (a-c) and physiological equivalent temperature (d-e) for all the simulated
609 summer days, i.e. reference past, 2020, 2050, and 2100, at 8 a.m. (a,d), 12 p.m. (b,e), and 4 p.m. (c,f).

611 12.00 p.m. and 4.00 p.m. result are the most critical moments in terms apparent temperature index
612 and consequentially for outdoors and recreational activities. In detail, a linear increasing in human
613 thermal discomfort is depicted from the reference scenario to the future scenarios. 2100 is expected

614 to be the most hazardous year due to overheating risk. In fact, the maximum value of AT is predicted
615 in 2100 and it is equal to 42°C, which means very hot sensation and huge level of psychological
616 stress. Spatially, the outcomes show a non-uniform distribution, in particular at 12.00 p.m. on 2020
617 and 2050 low values of AT are expected in the main square area. This fact can be imputable to the
618 wind speed contribution which decreases the air temperature values perception. Moreover, the
619 apparent temperature index is calculated by neglecting the direct global radiation contribution that
620 strictly influences human well-being in open field areas.

621 To fill this gap, the PET index is also calculated to have a more realistic thermal sensation forecast.
622 As can be seen in Figure 11, even PET outcomes show that 12:00 p.m. and 4:00 p.m. are the most
623 risky time of the day. 2100 is revealed to be the worst forecasted year in terms of human thermal
624 perception. From a spatial point of view, directly irradiated areas of the main square are revealed
625 to be exposed to the greatest risk of overheating.

626

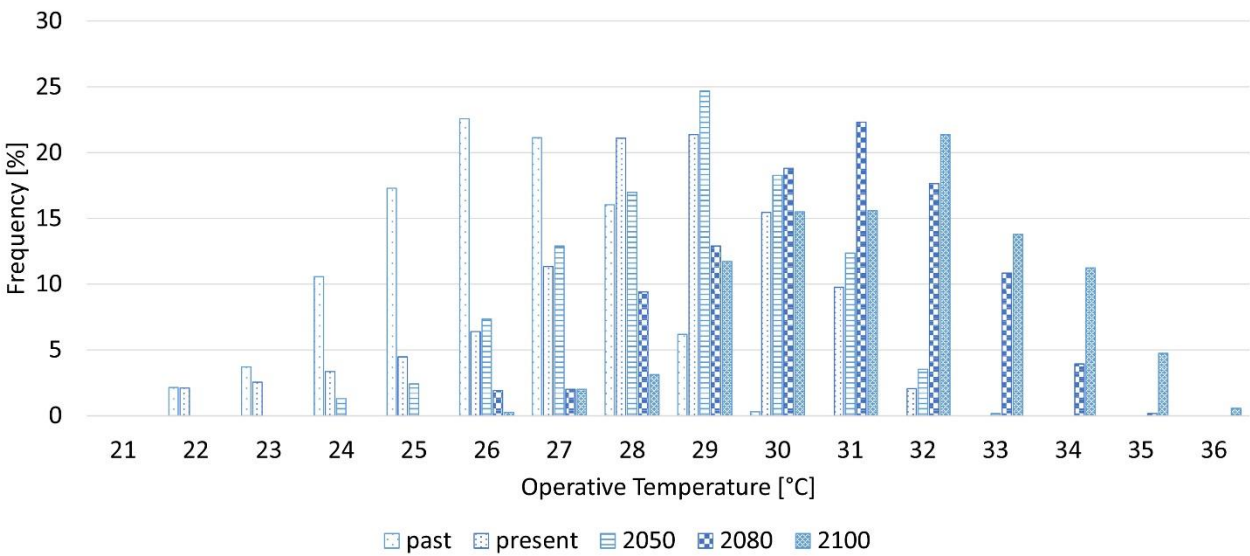
627 *4.4 Indoor thermal comfort perception: actual conditions and future forecast*

628 Crossing the building heritage envelope, here the focus is to understand climate change related
629 impact in the indoors of the key building of the historical city under investigation. To this aim, as
630 mentioned, the dynamic simulation model has been run under the same depicted scenarios, i.e. the
631 past, the reference, the 2020, the 2050 and the 2100. Figure 12 shows the operative temperature
632 hourly frequency outcomes obtained at these boundary timings in summer. In particular, the
633 simulated period extends from June 21st to September 21st and it is the most vulnerable period for
634 human thermal discomfort perception, both in indoors and outdoors.

635 As can be seen In Figure 12, in the current scenario the operative temperature exceeds 25°C which
636 is the maximum value allowed to have a thermal comfortable perception in offices environments,

637 according to the EN 15251 [47]. The histogram shows that 28°C and 29°C valued indeed present the
638 highest frequency in the current scenario. In the future, the operative temperature frequency is
639 forecast to increase up to 29°C. On 2050 the operative temperature value of 29°C is expected to be
640 repeated for more than 500 hours during the summer period during the course of the day, while in
641 2080 the most frequent operative temperature is foreseen to be equal to 30°C, reaching the
642 dangerous threshold temperature for most of the time. 2100 is predicted to be even worse, because
643 the average frequency of operative temperature expected will be 32°C and further peaks at 36°C
644 will be expected, which means great level of human thermal discomfort and, in general, lack of
645 livability in the indoors without HVAC systems operating, and high level of psychological stress for
646 tourists and dwellers in general.

647



648

649 *Figure 12.* Frequency distribution of obtained hourly operative temperature during summer for all the foreseen scenario simulated.

650

651 **1. Discussion**

652 The focus of the presented research consists of identifying the human perspective in the urban
653 environment affected by anthropogenic actions, responsible for local climate change and air quality
654 damaging. In this view, wearable sensing techniques and microclimate modelling provided a reliable
655 and novel coupled techniques aimed at defining the current and future situation, and its
656 responsibility on building energy need, cultural heritage conservation and, in general,
657 environmental analysis at citizens' level, for better resilient cities and outdoors. In fact, climate
658 change demonstrated to produce an undeniable impact on the total environment, cities and society
659 in terms of human wellbeing and, in most of ancient European cities, it is responsible for heavy
660 tourism drawbacks due to overheating, also impacting the economic sustainability of cultural
661 heritage sites and, more in general, their resilience. Cultural sites are heavily affected by climate
662 change related events, i.e. Urban Heat Island and overheating risk, since the great number of
663 mitigation strategies studied and exploited in the field are often inapplicable in historical city centers
664 due to cultural value preservation constraints. In this context, climate change evaluation and its
665 future progress prediction are crucial to identify outdoor and indoor thermal critical conditions for
666 humans, and to manage tourist flows in thermally comfortable areas of the city improving the urban
667 visitability and guaranteeing their resilience. Therefore, this manuscript proposes an innovative
668 methodology, specifically implemented in the field, with the purpose to investigate historical urban
669 outdoor and indoor conditions coupling extensive and multidimensional experimental monitoring
670 with calibrated numerical modeling of the indoor and outdoor dynamics. In more detail, the climate
671 survey monitoring campaign conducted by fixed weather station, small probes and an innovative
672 wearable system highlights how the climate monitoring scale influences the microclimate analysis
673 and the capability to detect microclimatic variability within the urban context, mostly responsible
674 for outdoor societal life and economic activities. More specifically, fixed weather station data allow
675 to have an annual and seasonal trend of the main environmental parameters, such as air

676 temperature and relative humidity, but are not able to catch the microclimate variability that
677 characterize complex heterogeneous urban environment. To this aim the climate survey scale can
678 be reduced and therefore two stand-alone small probes are located in neighboring areas
679 highlighting key differences between the two selected areas in terms of air temperature and relative
680 humidity values. However, a detailed monitoring campaign by wearable system is fundamental to
681 have the pedestrian perspective and assess the human outdoor thermal comfort throughout the
682 city, at the required small granularity affecting outdoor societal activities in the hotter seasons. On
683 the other hand, future climate change scenarios are then necessary in order to predict the evolution
684 of such microclimate and mesoclimate conditions in the near future. That is the reason why, each
685 indoor and outdoor validated model may be run also with varying boundary conditions, according
686 to any future prediction of climate change. For the purpose of this paper, the A2 scenario elaborated
687 by the IPCC has been selected as the most reliable one in the last years. Therefore, overheating risk
688 may be assessed in both the indoors and outdoors, preparing the ground for any multidisciplinary
689 assessment such as the economic investigation of climate change related issues produced on local
690 tourism activity and so on. The same may be investigated in the indoors where museum spaces or
691 new operations take place, which can be compromised by climate change progress even in the near
692 future. In fact, it is very much clear that starting from the next decades, the most probable indoor
693 operative temperature is higher than 29°C, exacerbating indoor overheating risks for employees and
694 tourists. In this view, the granular field monitoring data, coupled to microclimate modelling and
695 prediction of climate change, represented a novel, multiscale and integrated method for
696 investigating cultural heritage resilience to climate change, in terms of conservation boundaries,
697 visitability and wellbeing of tourists, representing a key motivation to keep cultural heritage areas
698 more livable and economically sustainable. Data granularity allowed indeed to frame real
699 pedestrians' boundary conditions affecting personal feelings and behaviors, and climate change

700 prediction allowed to frame this anthropogenic forcing toward a future perspective, which should
701 be considered when designing cultural heritage conservation and urban planning actions. Compared
702 to only simulation based works, or building-oriented works, the key add on produced through this
703 research consisted on the human-centric approach in defining indoor-outdoor wellbeing from
704 people perspective, where people (e.g. citizens and tourists) represent the key resilience and
705 economic resource for preserving cultural heritage sites and keeping their livability along the time.

706

707 **2. Conclusion**

708 The proposed multidimensional and multifunctional procedure has been applied on the Medieval
709 City of Gubbio, in central Italy. The field monitoring, conducted at different scales, highlights
710 progressively microclimate peculiarities of the monitored environment. In particular, different air
711 temperature profiles are collected by the two measurement points within the same historic center.
712 These results are explained considering different wind fields and different solar radiation access
713 within the two zones. The pedestrian perspective is deepened during a heat wave event in summer,
714 by means of a wearable environmental monitoring station. Moreover, future weather forecast
715 scenarios are simulated and the obtained output shows that in summer, from the past scenario to
716 the future scenario on 2100, a linear overheating in terms of air temperature and a non-linear trend
717 in terms of relative humidity. Moreover, the model of Palazzo dei Consoli is run under the same
718 scenarios and the results are reported in term of hourly operative temperature frequency for each
719 summer period. The outcomes show that in the future, the value of the most frequent indoor
720 operative temperature will increase from 29°C (today) up to 32°C on 2100, with peaks at 36°C in
721 2100, which means high level of thermal discomfort. Moreover, to investigate the human thermal
722 perception, two thermal indexes are calculated by taking into account the environmental
723 parameters collected by the wearable system and the weather condition foreseen according to the

724 IPCC prevision. South-facing spaces and highest sky-view-factor areas are shown to be the most
725 critical areas for citizens or tourists visiting the city in the central hours of the day. Outdoor comfort
726 indexes (apparent temperature) are computed for the predicted future scenarios coupled to the
727 calculation of the rational comfort index physiological equivalent temperature, i.e. PET. The
728 apparent temperature outcomes demonstrate that 12.00 p.m. and 4.00 p.m. are the most critical
729 moments of the day, i.e. 42°C, and a linear increasing in human thermal discomfort is depicted from
730 the past to the future 2100, which is expected to be the most hazardous time. The PET results
731 confirmed this trend and they highlighted the spatial variability of the values, with peaks higher than
732 50°C, highlighted that the main square of the city – the key tourism and citizenship attraction
733 position – is exposed to the greatest risk of overheating.

734 Concluding, the proposed analysis procedure and application to a field study demonstrated to
735 prepare a useful ground to understand the human perception both in indoors and outdoors within
736 cultural heritage places affected by climate change. Moreover, these considerations could help
737 different categories of end users, such as ministries, local governmental bodies, municipalities,
738 environmental protection agencies, etc. Intra-urban microclimate analysis by means of wearable
739 sensing techniques and numerical modelling may be of key help to better manage and preserve
740 tourism flows and local citizens' wellbeing, e.g. their societal attitudes and community belonging
741 feeling, towards more comfortable outdoor and indoor areas, in order to reduce the human health
742 hazard and to preserve local customs and traditions.

743

744 **ACKNOWLEDGEMENTS**

745 Acknowledgements are due to the European Union's Horizon 2020 program under grant agreement
746 No 678407 (ZERO-PLUS) and n° 700395 (HERACLES). The authors also thank UNESCO Chair on

747 “Water Resources Management and Culture”, and the Honors Center of Italian Universities (H2CU)
748 for supporting their studies on cultural heritage. Additionally, the first author is supported by
749 Ministry funding and university funding of the PhD school in Energy and Sustainable Development.
750 Dr. Piselli wishes to thank Regione Umbria and Department of Engineering at UNIPG for supporting
751 the project "SMEET-WELL: SMart building managEment for Energy saving meets WELLbeing".

752

753 **REFERENCES**

754 [1] D. Mitchell, C. Heaviside, S. Vardoulakis, C. Huntingford, G. Masato, B. P Guillod, P.
755 Frumhoff, A. Bowery, D. Wallom, and M. Allen, “Attributing human mortality during
756 extreme heat waves to anthropogenic climate change,” *Environ. Res. Lett.*, vol. 11, no. 7,
757 2016.

758 [2] L. Nicholls and Y. Strengers, “Heatwaves, cooling and young children at home: Integrating
759 energy and health objectives,” *Energy Res. Soc. Sci.*, vol. 39, no. September 2017, pp. 1–9,
760 2018.

761 [3] G. A. Meehl and C. Tebaldi, “More intense, more frequent, and longer lasting heat waves in
762 the 21st century,” *Science (80-.)*, vol. 305, no. 5686, pp. 994–997, 2004.

763 [4] M. Santamouris, L. Ding, F. Fiorito, P. Oldfield, P. Osmond, R. Paolini, D. Prasad, and A.
764 Synnefa, “Passive and active cooling for the outdoor built environment – Analysis and
765 assessment of the cooling potential of mitigation technologies using performance data from
766 220 large scale projects,” *Sol. Energy*, vol. 154, pp. 14–33, 2017.

767 [5] I. Agathangelidis, C. Cartalis, M. Santamouris, I. Agathangelidis, C. Cartalis, and M.
768 Santamouris, “Integrating Urban Form, Function, and Energy Fluxes in a Heat Exposure

- 769 Indicator in View of Intra-Urban Heat Island Assessment and Climate Change Adaptation,”
770 *Climate*, vol. 7, no. 6, p. 75, May 2019.
- 771 [6] R. Paolini, F. Antretter, F. Cotana, A. L. Pisello, M. MeshkinKiya, A. Zani, T. Poli, and V. L.
772 Castaldo, “The hygrothermal performance of residential buildings at urban and rural sites:
773 Sensible and latent energy loads and indoor environmental conditions,” *Energy Build.*, vol.
774 152, pp. 792–803, 2016.
- 775 [7] H. Gilbert, B. H. Mandel, and R. Levinson, “Keeping California cool: Recent cool community
776 developments,” *Energy Build.*, vol. 114, pp. 20–26, Feb. 2016.
- 777 [8] M. Masoudi and P. Y. Tan, “Multi-year comparison of the effects of spatial pattern of urban
778 green spaces on urban land surface temperature,” *Landsc. Urban Plan.*, vol. 184, pp. 44–58,
779 Apr. 2019.
- 780 [9] M. Santamouris, “On the energy impact of urban heat island and global warming on
781 buildings,” *Energy Build.*, vol. 82, pp. 100–113, 2014.
- 782 [10] S. E. Perkins, L. V Alexander, and J. R. Nairn, “Increasing frequency, intensity and duration of
783 observed global heatwaves and warm spells,” *Geophys. Res. Lett.*, vol. 39, no. 20, 2012.
- 784 [11] D. Li and E. Bou-Zeid, “Synergistic interactions between urban heat islands and heat waves:
785 The impact in cities is larger than the sum of its parts,” *J. Appl. Meteorol. Climatol.*, vol. 52,
786 no. 9, pp. 2051–2064, 2013.
- 787 [12] I. Livada, A. Synnefa, S. Haddad, R. Paolini, S. Garshasbi, G. Ulpiani, F. Fiorito, K.
788 Vassilakopoulou, P. Osmond, and M. Santamouris, “Time series analysis of ambient air-
789 temperature during the period 1970–2016 over Sydney, Australia,” *Sci. Total Environ.*, vol.
790 648, pp. 1627–1638, 2019.

- 791 [13] M. Santamouris, N. Papanikolaou, I. Livada, I. Koronakis, C. Georgakis, A. Argiriou, and D. N.
792 Assimakopoulos, "On the impact of urban climate on the energy consumption of building,"
793 *Sol. Energy*, vol. 70, no. 3, pp. 201–216, 2001.
- 794 [14] J. Huang and K. R. Gurney, "Impact of climate change on U.S. building energy demand:
795 Financial implications for consumers and energy suppliers," *Energy Build.*, vol. 139, pp. 747–
796 754, 2017.
- 797 [15] A. J. McMichael, R. E. Woodruff, and S. Hales, "Climate change and human health: Present
798 and future risks," *Lancet*, vol. 367, no. 9513, pp. 859–869, 2006.
- 799 [16] J. Rodríguez-Algeciras, A. Tablada, and A. Matzarakis, "Effect of asymmetrical street canyons
800 on pedestrian thermal comfort in warm-humid climate of Cuba," *Theor. Appl. Climatol.*, vol.
801 133, no. 3–4, pp. 663–679, 2018.
- 802 [17] S. S. Abed and A. Matzarakis, "Quantification of the Tourism Climate of Algeria based on the
803 climate-tourism-information-scheme," *Atmosphere (Basel)*, vol. 9, no. 7, 2018.
- 804 [18] F. Salata, I. Golasi, R. Proietti, and A. de Lieto Vollaro, "Implications of climate and outdoor
805 thermal comfort on tourism: the case of Italy," *Int. J. Biometeorol.*, 2017.
- 806 [19] R. Freeman and M. Yearworth, "Climate change and cities: problem structuring methods
807 and critical perspectives on low-carbon districts," *Energy Res. Soc. Sci.*, vol. 25, pp. 48–64,
808 2017.
- 809 [20] M. Santamouris, "Using cool pavements as a mitigation strategy to fight urban heat island -
810 A review of the actual developments," *Renew. Sustain. Energy Rev.*, vol. 26, pp. 224–240,
811 2013.
- 812 [21] F. Rossi, F. Cotana, M. Filippini, A. Nicolini, S. Menon, and A. Rosenfeld, "Cool roofs as a

- 813 strategy to tackle global warming: economical and technical opportunities," *Adv. Build.*
814 *Energy Res.*, vol. 7, no. 2, pp. 254–268, 2013.
- 815 [22] A. H. Rosenfeld, H. Akbari, J. J. Romm, and M. Pomerantz, "Cool communities: Strategies for
816 heat island mitigation and smog reduction," *Energy Build.*, vol. 28, no. 1, pp. 51–62, 1998.
- 817 [23] A. L. Pisello, E. Fortunati, C. Fabiani, S. Mattioli, F. Dominici, L. Torre, L. F. Cabeza, and F.
818 Cotana, "PCM for improving polyurethane-based cool roof membranes durability," *Sol.*
819 *Energy Mater. Sol. Cells*, vol. 160, pp. 34–42, 2017.
- 820 [24] A. de Gracia, L. Navarro, J. Coma, S. Serrano, J. Romaní, G. Pérez, and L. F. Cabeza,
821 "Experimental set-up for testing active and passive systems for energy savings in buildings –
822 Lessons learnt," *Renew. Sustain. Energy Rev.*, vol. 82, pp. 1014–1026, 2018.
- 823 [25] J. Coma, G. Pérez, A. de Gracia, S. Burés, M. Urrestarazu, and L. F. Cabeza, "Vertical
824 greenery systems for energy savings in buildings: A comparative study between green walls
825 and green facades," *Build. Environ.*, vol. 111, pp. 228–237, 2017.
- 826 [26] G. Pérez, J. Coma, S. Sol, and L. F. Cabeza, "Green facade for energy savings in buildings: The
827 influence of leaf area index and facade orientation on the shadow effect," *Appl. Energy*, vol.
828 187, pp. 424–437, 2017.
- 829 [27] M. Santamouris, "Cooling the cities - A review of reflective and green roof mitigation
830 technologies to fight heat island and improve comfort in urban environments," *Sol. Energy*,
831 vol. 103, pp. 682–703, 2014.
- 832 [28] M. F. Shahidan, P. J. Jones, J. Gwilliam, and E. Salleh, "An evaluation of outdoor and building
833 environment cooling achieved through combination modification of trees with ground
834 materials," *Build. Environ.*, vol. 58, pp. 245–257, 2012.

- 835 [29] J. Xu, Q. Wei, X. Huang, X. Zhu, and G. Li, "Evaluation of human thermal comfort near urban
836 waterbody during summer," *Build. Environ.*, vol. 45, no. 4, pp. 1072–1080, 2010.
- 837 [30] V. L. Castaldo, F. Rosso, I. Golasi, C. Piselli, F. Salata, A. L. Pisello, M. Ferrero, F. Cotana, and
838 A. De Lieto Vollaro, "Thermal comfort in the historical urban canyon: The effect of
839 innovative materials," in *Energy Procedia*, 2017, vol. 134, pp. 151–160.
- 840 [31] G. Leijonhufvud and A. Henning, "Rethinking indoor climate control in historic buildings: The
841 importance of negotiated priorities and discursive hegemony at a Swedish museum,"
842 *Energy Res. Soc. Sci.*, vol. 4, no. C, pp. 117–123, 2014.
- 843 [32] A. L. Pisello, A. Petrozzi, V. L. Castaldo, and F. Cotana, "On an innovative integrated
844 technique for energy refurbishment of historical buildings: Thermal-energy, economic and
845 environmental analysis of a case study," *Appl. Energy*, vol. 162, pp. 1313–1322, 2014.
- 846 [33] R. Oliveira, J. Lopes, H. Sousa, and M. Abreu, "A system for the management of old building
847 retrofit projects in historical centres: the case of Portugal," *Int. J. Strateg. Prop. Manag.*, vol.
848 21, no. 2, pp. 199–211, Apr. 2017.
- 849 [34] L. Chen and E. Ng, "Outdoor thermal comfort and outdoor activities: A review of research in
850 the past decade," *Cities*, vol. 29, no. 2, pp. 118–125, 2012.
- 851 [35] K. Rashidi, M. Stadelmann, and A. Patt, "Creditworthiness and climate: Identifying a hidden
852 financial co-benefit of municipal climate adaptation and mitigation policies," *Energy Res.*
853 *Soc. Sci.*, vol. 48, no. October 2018, pp. 131–138, 2019.
- 854 [36] O. Potchter, P. Cohen, T.-P. Lin, and A. Matzarakis, "Outdoor human thermal perception in
855 various climates: A comprehensive review of approaches, methods and quantification," *Sci.*
856 *Total Environ.*, vol. 631–632, pp. 390–406, 2018.

- 857 [37] M. Kottek, J. Grieser, C. Beck, B. Rudolf, and F. Rubel, "World map of the Köppen-Geiger
858 climate classification updated," *Meteorol. Zeitschrift*, vol. 15, no. 3, pp. 259–263, 2006.
- 859 [38] I. Pigliautile and A. L. Pisello, "A new wearable monitoring system for investigating
860 pedestrians' environmental conditions: Development of the experimental tool and start-up
861 findings," *Sci. Total Environ.*, vol. 630, 2018.
- 862 [39] F. Salata, I. Golasi, R. de Lieto Vollaro, and A. de Lieto Vollaro, "Urban microclimate and
863 outdoor thermal comfort. A proper procedure to fit ENVI-met simulation outputs to
864 experimental data," *Sustain. Cities Soc.*, vol. 26, pp. 318–343, 2016.
- 865 [40] G. Battista, E. Carnielo, and R. De Lieto Vollaro, "Thermal impact of a redeveloped area on
866 localized urban microclimate: A case study in Rome," *Energy Build.*, vol. 133, pp. 446–454,
867 2016.
- 868 [41] M. Bruse and H. Fleer, "Simulating surface-plant-air interactions inside urban environments
869 with a three dimensional numerical model," *Environ. Model. Softw.*, vol. 13, no. 3–4, pp.
870 373–384, 1998.
- 871 [42] R. Taesler and C. Andersson, "A method for solar radiation computations using routine
872 meteorological observations," *Energy Build.*, vol. 7, no. 4, pp. 341–352, 1984.
- 873 [43] A. Zhang, R. Bokel, A. van den Dobbelsteen, Y. Sun, Q. Huang, and Q. Zhang, "An integrated
874 school and schoolyard design method for summer thermal comfort and energy efficiency in
875 Northern China," *Build. Environ.*, vol. 124, pp. 369–387, 2017.
- 876 [44] V. L. Castaldo, A. L. Pisello, I. Pigliautile, C. Piselli, and F. Cotana, "Microclimate and air
877 quality investigation in historic hilly urban areas: Experimental and numerical investigation
878 in central Italy," *Sustain. Cities Soc.*, vol. 33, 2017.

- 879 [45] D. B. Crawley, C. O. Pedersen, L. K. Lawrie, and F. C. Winkelmann, "Energy plus: Energy
880 simulation program," *ASHRAE J.*, vol. 42, pp. 49–56, 2000.
- 881 [46] UK Department for Communities and Local Government (DCLG), "UK's National Calculation
882 Method for Non Domestic Buildings," 2004. .
- 883 [47] "EN 15251:2007 - Indoor Environmental Input Parameters for Design and Assessment of
884 Energy Performance of Buildings Addressing Indoor Air Quality, Thermal Environment,
885 Lighting and Acoustics." 2007.
- 886 [48] C. A. Gueymard and D. R. Myers, "Validation and Ranking Methodologies for Solar Radiation
887 Models BT - Modeling Solar Radiation at the Earth's Surface: Recent Advances," V. Badescu,
888 Ed. Berlin, Heidelberg: Springer Berlin Heidelberg, 2008, pp. 479–510.
- 889 [49] J. E. Hay, "Calculation of monthly mean solar radiation for horizontal and inclined surfaces,"
890 *Sol. Energy*, vol. 23, no. 4, pp. 301–307, 1979.
- 891 [50] G. Emmi, R. Perego, S. Pera, M. De Carli, M. Cultrera, D. Mendrinios, S. Graci, A. Di Bella, R.
892 Pasquali, A. Zarrella, A. Galgaro, G. Mezzasalma, G. Dalla Santa, and A. Bernardi, "A
893 Database for Climatic Conditions around Europe for Promoting GSHP Solutions,"
894 *Geosciences*, vol. 8, no. 2, p. 71, 2018.
- 895 [51] IPCC, "Climate Change 2013," 2013.
- 896 [52] Intergovernmental Panel on Climate Change, Ed., "Summary for Policymakers," in *Climate*
897 *Change 2013 – The Physical Science Basis: Working Group I Contribution to the Fifth*
898 *Assessment Report of the Intergovernmental Panel on Climate Change*, Cambridge:
899 Cambridge University Press, 2014, pp. 1–30.
- 900 [53] A. Matzarakis, F. Rutz, and H. Mayer, "Modelling radiation fluxes in simple and complex

901 environments: Basics of the RayMan model," *Int. J. Biometeorol.*, vol. 54, no. 2, pp. 131–
902 139, 2010.

903 [54] A. Matzarakis, F. Rutz, and H. Mayer, "Modelling the thermal bioclimate in urban areas with
904 the RayMan Model," *Energy*, vol. 6–8, Jan. 2006.

905 [55] R. G. Steadman, "A Universal Scale of Apparent Temperature," *J. Appl. Meteorol. - J APPL*
906 *METEOROL*, vol. 23, no. 12, pp. 1674–1687, Dec. 1984.

907 [56] Australian Government- Bureau of Meteorology, "Thermal Comfort observations," 2010. .

908 [57] R. G. Steadman, "Norms of Apparent Temperature in Australia," *Aust. Meteorol. Mag.*, vol.
909 43, pp. 1–16, Jan. 1994.

910 [58] H. PR, "The physiological equivalent temperature - A universal index for the
911 biometeorological assessment of the thermal environment," *Int. J. Biometeorol.*, vol. 43, no.
912 2, pp. 71–75, Nov. 1999.

913 [59] S. Cocco, J. Kämpf, J.-L. Scartezzini, and D. Pearlmutter, "Outdoor human comfort and
914 thermal stress: A comprehensive review on models and standards," *Urban Clim.*, vol. 18, pp.
915 33–57, 2016.

916 [60] P. Cohen, O. Potchter, and A. Matzarakis, "Human thermal perception of Coastal
917 Mediterranean outdoor urban environments," *Appl. Geogr.*, vol. 37, no. 1, pp. 1–10, 2013.

918 [61] A. Matzarakis, F. Rutz, and H. Mayer, "Modelling radiation fluxes in simple and complex
919 environments - Application of the RayMan model," *Int. J. Biometeorol.*, vol. 51, no. 4, pp.
920 323–334, 2007.

921 [62] A. Pyrgou, V. L. Castaldo, A. L. Pisello, F. Cotana, and M. Santamouris, "Differentiating
922 responses of weather files and local climate change to explain variations in building

- 923 thermal-energy performance simulations,” *Sol. Energy*, vol. 153, pp. 224–237, 2017.
- 924 [63] A. Pyrgou, V. L. Castaldo, A. L. Pisello, F. Cotana, and M. Santamouris, “On the effect of
925 summer heatwaves and urban overheating on building thermal-energy performance in
926 central Italy,” *Sustain. Cities Soc.*, vol. 28, pp. 187–200, 2017.
- 927 [64] M. Belardi, *Il Palazzo dei consoli a Gubbio e il centro urbano trecentesco (in Italian)*. Perugia,
928 2001.
- 929